New Pathway for the $CH_3 + OH \rightarrow CH_2 + H_2O$ Reaction on a Triplet Surface

Craig Wilson* and Gabriel G. Balint-Kurti

School of Chemistry, University of Bristol, Bristol BS8 1TS, U.K.

Received: September 16, 1997; In Final Form: November 10, 1997

Using the methods of ab initio quantum chemistry, a new pathway has been identified for the gas-phase reaction of $CH_3 + OH \rightarrow CH_2 + H_2O$. The new pathway occurs on a potential energy surface corresponding to a triplet spin state of the overall system. The reaction, via this pathway, produces a ground-state, triplet methylene fragment and may be written as $CH_3(\tilde{X}^2A_2'') + OH(\tilde{X}^2\Pi_\Omega) \rightarrow CH_2(\tilde{X}^3B_1) + H_2O$. The transition state for this hydrogen abstraction has been calculated using second-order Møller−Plesset (MP2) perturbation theory. Higher level calculations at the geometry of the transition state yield an activation energy for the reaction of $E_a = 25.15$ kJ mol^{-1} at 0 K. A portion of the reaction path has been computed and has been used to calculated rate constants for the reaction. Rate constants were computed using both conventional transition-state theory and variational transition-state theory both with and without tunneling corrections. The predicted barrier to the reaction precludes the triplet-abstraction pathway from being important in the low-temperature reaction dynamics of the $CH_3 + OH$ system. Our predictions show, however, that, at the higher temperatures prevalent in hydrocarbon flames (1000−2200 K), the reaction will play an important role.

1. Introduction

The reaction of CH_3 with OH is known to play a significant role in the combustion mechanisms of almost all hydrocarbons. Many theoretical[1−5] and experimental[6−13] studies of the reaction have, accordingly, been carried out. On the singlet surface, the reaction is believed to occur via formation and subsequent decomposition (or stabilization) of vibrationally excited methanol. There are many possible product channels, and, for a complete description of the reaction, knowledge of the branching ratios into the various channels is required. In particular, it is important to assess the relative importance of channels that produce reactive radicals and those that produce stable species. Some of the more important channels are shown below:

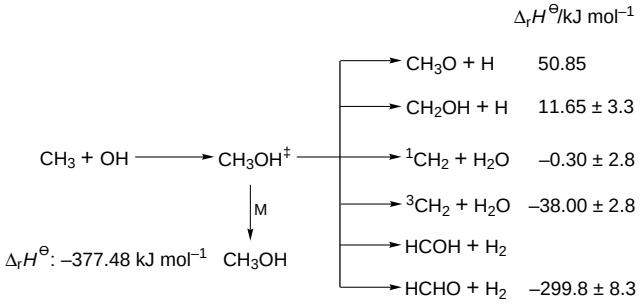

The reaction enthalpies are given at 0 K and were calculated from thermodynamic data given in Table 1.

Experimentally determined rate constants and branching ratios for most of these channels have been reported in the literature. Hack et al.[6] used laser photolysis/laser-induced fluorescence methods to study the reaction of singlet CH_2 (denoted henceforth as $^1CH_2$) with H_2O, one channel of which leads to $CH_3 + OH$, i.e., the reverse reaction to the title reaction. By estimating an equilibrium constant from thermodynamic data, they were able to report a rate constant of $k^{298} \approx 3 \times 10^{-11}$ cm^3 s^{-1} for the $CH_3 + OH \rightarrow {}^1CH_2 + H_2O$ reaction. A later study by Oser et al.[8] using a fast-flow technique detected production of H_2O directly and reported of $k^{300} \leq 5 \times 10^{-12}$ cm^3 s^{-1}. A similar study by the same authors[9,10] using deuterated OH gave $k^{300} = 1 \times 10^{-12}$ cm^3 s^{-1}. The value reported by Hack et al.[6] was held to be in error[9] because of uncertainties in the thermodynamic data used to estimate the rate constant. While current evidence certainly casts doubt on the very high value of the rate constant reported by Hack et al.[6] for the singlet reaction, it should be noted that the spectroscopy-based experimental techniques used in the work of refs 6 and 7 are the only ones of those used so far that are able to distinguish between a reaction on the singlet and triplet surface. The rate constants reported in refs 8−10 rely on the computer modeling of CH_3 falloff behavior. As the title reaction of this paper was not included in the modeling, there is no way in which the triplet (1) and singlet (2) reactions

TABLE 1: Standard Enthalpies of Formation at 0 K

	$\Delta_f H^\ominus$/kJ mol^{-1}	source
CH_3	149.031 ± 0.8	ref 14
OH	38.75 ± 1.21[a]	ref 14
$^3CH_2$	388.7 ± 0.7	ref 16
$^1CH_2$	426.4 ± 0.7	ref 16
H_2O	−238.921 ± 0.042	ref 14
HCHO	−112.057 ± 6.3	ref 14
H_2	0.0	
CH_3O	22.6	ref 15
CH_2OH	−16.6 ± 1.3[b]	ref 16
CH_3OH	−189.7	ref 15
H	216.035 ± 0.006	ref 14

[a] This value is taken from the text where it is reported to be 9.261 kcal mol^{-1} (38.75 kJ mol^{-1}). A different number (38.39 kJ mol^{-1}) is reported at the top of the page. [b] This is the enthalpy of formation at 298 K.

$$CH_3(\tilde{X}^2A_2'') + OH(\tilde{X}^2\Pi_\Omega) \rightarrow CH_2(\tilde{X}^3B_1) + H_2O$$

or

$$^2CH_3 + {}^2OH \rightarrow {}^3CH_2 + H_2O \quad (1)$$

S1089-5639(97)03026-0 CCC: $15.00
Published on Web 02/11/1998

and

$$^2CH_3 + {}^2OH \rightarrow {}^1CH_2 + H_2O \qquad (2)$$

can be distinguished in the reported experiments.

A theoretical study by Walch[2] showed that the channel $CH_3 + OH \rightarrow {}^1CH_2 + H_2O$ had no activation barrier. Given that thermodynamic data[14,17] indicate that the singlet reaction (2) should be almost thermoneutral, it is clearly of importance in the $CH_3 + OH$ reaction. The singlet−triplet splitting of CH_2 is now known to be 37.648 ± 0.059 kJ mol^{-1},[18] which means that the reaction of CH_3 with OH on a *triplet* surface to form $^3CH_2$ and H_2O is exothermic

$$CH_3 + OH \rightarrow {}^3CH_2 + H_2O$$
$$\Delta_r H^{\ominus} = -38.00 \pm 2.8 \text{ kJ mol}^{-1}$$

where $\Delta_r H^{\ominus}$ is the standard enthalpy of formation at 0 K.

The reaction on the triplet surface is a direct hydrogen abstraction by OH and does not involve formation of a methanol complex as an intermediate step. As far as we are aware, this reaction has not been studied experimentally. One theoretical study by Dean and Westmoreland[1] briefly mentioned the possibility of this channel occurring. They estimated a rate constant using data from other reactions of $^3CH_2$. Their estimate showed that this channel would be unimportant except at high temperatures (>1500 K). Such temperatures do occur in methane combustion. To our knowledge, there have been no previous thorough studies of this potentially important reaction channel.

For a system with as many degrees of freedom as the current one, it is not possible to undertake a full quantum mechanical treatment of the reaction dynamics. Even a classical mechanical treatment requires a knowledge of large regions of the potential energy surface that are expensive to compute. Transition-state theory approaches[19] require only a knowledge of the transition-state region of the potential and possibly of a small region of the reaction path close to it. Our approach is therefore to use sophisticated quantum chemical electronic structure methods to locate the transition-state geometry and then to calculate energies and vibrational force fields along a reaction pathway. This information can then be used to perform a transition-state theory calculation of the rate constant for the reaction. In the body of the paper below we report such calculations and our best estimates of the rate constant for the reaction on the triplet surface.

2. Electronic Structure Calculations

Electronic structure calculations were carried out using the programs Gaussian 94[20] and Molpro 96[21]on a Silicon Graphics Origin 200 and a Silicon Graphics Power Challenge XL at this university and on a Digital 8400 and a Cray J90 at the Rutherford-Appleton Laboratory. Geometry optimizations were performed using second-order Møller−Plesset[22] (MP2) perturbation theory and a correlation-corrected double-ζ plus valence polarization basis[23] (cc-pvdz) on the reactants and products of the reaction. A search for a transition state on the triplet surface was carried out at the same level of theory. Once this had been located, normal-mode analyses were performed on all species. A calculation that followed the minimum-energy path (MEP) down from the transition state in both directions (known as an IRC calculation in Gaussian) was also performed. This confirmed that the transition state linked the desired reactants and products. The calculation also gave the geometries of points on the minimum-energy reaction path (MEP) that were used to set up the variational transition-state (VTST) calculations (see below). Further single-point calculations at the MP2 transition-state geometries were performed to obtain improved energetics for the reaction. These were at the fourth-order Møller−Plesset (MP4)[22] level with the cc-pvtz basis set and the larger 6-311+G-(2df,p) basis set,[24] and at the Quadratic CI (QCISD(T))[25] level with the cc-pvdz, cc-pvtz, and cc-pvqz basis sets.

In addition, a multireference configuration interaction (MRCI) approach to the problem was used to try to obtain accurate variational energies to compare with those obtained from the QCISD(T) calculations. For the reactants, products, and transition state, symmetry-restricted Hartree−Fock ROHF/cc-pvdz calculations (using Molpro) were carried out at the optimized MP2 geometries. The ROHF orbitals were examined, and, on the basis of these orbitals, an active space for a CASSCF[26] calculation was chosen. The active space chosen consisted of six electrons in six orbitals. At the transition state (triplet multiplicity), these orbitals were bonding orbitals associated with the breaking C−H bond and the forming O−H bond and the orbitals containing the unpaired electrons. CASSCF calculations were performed using the vdz, vtz and vqz basis sets. Following each of these calculations, a multireference configuration interaction calculation (MR-CISD)[27] was performed using all the configurations from the CASSCF as reference functions. The resulting MR-CISD energies were corrected for size consistency using the multireference analogue of the Davidson correction. In addition, full-valence CASSCF calculations were carried out using the vdz, vtz, and vqz basis sets. In all of the

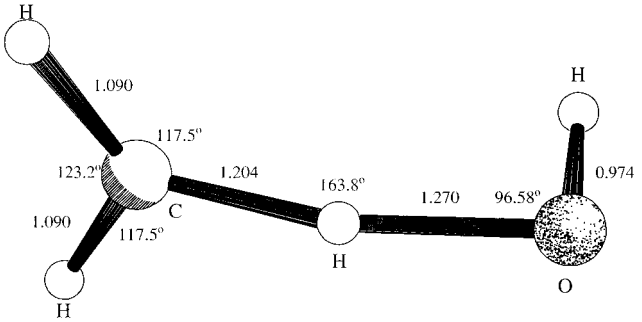

Figure 1. Schematic diagram of the transition-state geometry for $CH_3 + OH \rightarrow CH_2 + H_2O$ on the triplet surface.

TABLE 2: Geometrical Parameters for the Transition State, As Calculated at the MP2/cc-pvdz Level

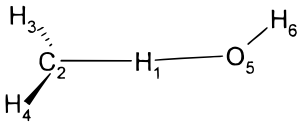

bond lengths/Å	bond angles/deg	dihedral angles/deg
$r_{12} = 1.204$	$a_{123} = 117.50$	$d_{4213} = 194.8$
$r_{23} = 1.090$	$a_{124} = 117.50$	$d_{5123} = 262.6$
$r_{24} = 1.090$	$a_{215} = 163.78$	$d_{6512} = 0.0$
$r_{15} = 1.270$	$a_{156} = 96.58$	
$r_{56} = 0.974$		

TABLE 3: Vibrational Frequencies of $H_2C-H-OH$ at Transition-State Geometry

vibrational frequency/cm^{-1}	vibrational frequency/cm^{-1}
−1919.3	1185.1
150.0	1259.8
275.0	1377.0
448.8	3226.3
519.2	3391.9
901.1	3800.3

TABLE 4: Electronic Energies Calculated Using the MP2 and MP4(SDTQ) Methods[a]

	MP2/cc-pvdz	MP4/cc-pvtz	MP4/6-311+G(2df,p)	zero-point correction[b]
CH_3	−39.693 089	−39.775 064	−39.770 924	0.030 101
OH	−75.544 867	−75.649 344	−75.651 118	0.008 643
$^3CH_2$	−39.021 781	−39.089 976	−39.089 531	0.017 792
H_2O	−76.230 989	−76.346 531	−76.344 602	0.021 663
transition state	−115.223 543	−115.412 109	−115.407 879	0.037 669
ΔE_r/kJ mol^{-1}	−38.89	−31.77	−31.74	1.87
$\Delta_r H^\ominus$/kJ mol^{-1}	−37.03	−29.90	−29.88	N/A
$\Delta E^\ddagger$/kJ mol^{-1}	37.84	32.29	37.18	−2.82
$E_a°$/kJ mol^{-1}	35.02	29.47	34.36	N/A

[a] Energy units are in Hartrees in the upper half of the table and in kJ mol^{-1} in the lower half. [b] Calculated at the MP2/cc-pvdz level.

TABLE 5: Electronic Energies Calculated Using the QCISD(T) Method[a]

	QCISD(T)/6-311+G(2df,p)	QCISD(T)/cc-pvdz	QCISD(T)/ cc-pvtz	QCISD(T)/cc-pvqz	zero-point correction[b]
CH_3	−39.772 244	−39.718 622	−39.776 397	−39.801 488	0.030 101
OH	−75.651 950	−75.561 208	−75.650 110	−75.692 090	0.008 643
$^3CH_2$	−39.091 183	−39.043 690	−39.091 636	−39.115 319	0.017 792
H_2O	−76.343 814	−76.243 467	−76.345 812	−76.391 043	0.021 663
transition state	−115.411 782	−115.266 570	−115.415 779	−115.482 924	0.037 669
ΔE_r/kJ mol^{-1}	−28.36	−19.24	−28.73	−33.56	1.87
$\Delta_r H^\ominus$/kJ mol^{-1}	−26.50	−17.37	−26.86	−31.69	N/A
$\Delta E^\ddagger$/kJ mol^{-1}	32.59	34.81	28.17	27.97	−2.82
$E_a°$/kJ mol^{-1}	29.77	31.99	25.34	25.15	N/A

[a] Energy units are in Hartrees in the upper half of the table and in kJ mol^{-1} in the lower half. [b] Calculated at the MP2/cc-pvdz level.

TABLE 6: Electronic Energies Calculated Using the CASSCF Method

	CASSCF(6,6)/cc-pvdz	CASSCF(14,12)/cc-pvdz	CASSCF(14,12)/cc-pvtz	CASSCF(14,12)/cc-pvqz	zero-point correction[b]
reactants	−114.989 514	−115.033 653	−115.071 838	−115.081 415	0.038 744
products	−114.969 548	−115.040 561	−115.081 634	−115.092 226	0.039 455
transition state	−114.960 550	−115.008 572	−115.045 447	−115.054 630	0.037 669
ΔE_r/kJ mol^{-1}	52.42	−18.14	−25.72	−28.38	1.87
$\Delta_r H^\ominus$/kJ mol^{-1}	54.29	−16.27	−23.85	−26.51	N/A
$\Delta E^\ddagger$/kJ mol^{-1}	76.04	65.85	69.29	70.32	−2.82
$E_a°$/kJ mol^{-1}	73.22	63.03	66.47	67.50	N/A

[a] Energy units are in Hartrees in the upper half of the table and in kJ mol^{-1} in the lower half. [b] Calculated at the MP2/cc-pvdz level.

CASSCF and MRCI work, calculations for the reactants and the products were based on the "supermolecule" approach. The reactant molecules at their equilibrium MP2 geometries were placed at a separation of 1000 Å, and the appropriate calculation was carried out. A similar calculation was also performed for the products. In this way, consistency of the chosen active space was ensured.

2.A. Results. As reported above, a transition-state geometry for the reaction was located at the MP2/cc-pvdz level. The geometrical parameters for the transition state are given in Table 2, and Figure 1 shows a schematic diagram of the system in its transition-state geometry. The vibrational frequencies of the transition state calculated at the MP2 level are given in Table 3. The geometry of the transition state is exactly of the type that is expected in a straightforward abstraction reaction. The C−H bond that is about to break is stretched from its equilibrium geometry in CH_3 (by about 0.1 Å), and the newly forming H−O bond is also longer than it will eventually be in the H_2O product (by about 0.3 Å). These C−H and H−O distances show that the transition state is reactant-like; i.e. it occurs early along the reaction path, as is expected for an exothermic reaction. The fact that the system has a triplet spin symmetry does not seem to give rise to any unexpected features in the surface. Electronic energies for the reactants, transition state, and products at all the levels of theory employed are given in Tables 4−7. Also shown in these tables are the classical barrier heights ($\Delta E^\ddagger$) (which refer to 0 K and do not include the zero-point corrections); the Arrhenius activation energies at 0 K ($E_a°$) (which correspond to the barrier heights with inclusion of zero-point energy correction); the classical reaction energies (ΔE_r) and the reaction enthalpies at 0 K ($\Delta_r H^\ominus$). The zero-point energies were calculated from normal-mode analyses at the MP2/cc-pvdz level. Table 4 shows the energies calculated at the MP2 and MP4 levels, Table 5 energies at the QCISD(T) level, Table 6 energies computed using the CASSCF method, and Table 7 energies computed using the MRCI method. For the CASSCF, MRCI, and QCISD(T) calculations, the effect of increasing the basis set size progressively (vdz, vtz, vqz) can be seen from the tables. Figure 2 shows the convergence of the activation energy with increasing basis set size for the various methods, and Figure 3 shows the convergence of the reaction enthalpy.

It may clearly be seen from the tables and from Figure 2 that the full-valence CASSCF calculations give much higher activation energies than the MRCI or the QCI methods. The Møller−Plesset perturbation methods are not included in the figures as they are less reliable than the QCI method. The MRCI results agree fairly well with the QCISD(T) results for the activation energy. The inclusion of Davidson corrections for size consistency at the MRCI level was vital (see Table 7). These corrections reduced barrier heights predicted by the MRCI method by up to 10 kJ mol^{-1}. Importantly, it can be seen that at the QCISD(T) level, the activation energy has converged with respect to the size of the basis set. The lowest barrier height and reaction enthalpy were obtained at the QCISD(T) level of theory, which is a size-consistent method. The inclusion of triple excitations results in slightly lower reaction barriers and enthalpies when compared to the large CASSCF and MRCI calculations. The QCISD(T) calculations also gave a lower barrier height than the corresponding MP4 calculations (compare

TABLE 7: Electronic Energies Calculated Using the Multireference CI Method[a]

	MR-CISD/ cc-pvdz	MR-CISD/cc-pvdz + Davidson[b]	MR-CISD/ cc-pvtz	MR-CISD/cc-pvtz + Davidson[b]	MR-CISD/ cc-pvqz	MR-CISD/cc-pvqz + Davidson[b]	zero-point correction[c]
reactants	−115.253 810	−115.275 078	−115.364 653	−115.394 743	−115.396 221	−115.428 752	0.038 744
products	−115.256 511	−115.281 374	−115.369 130	−115.404 066	−115.401 653	−115.437 723	0.039 455
transition state	−115.238 056	−115.262 120	−115.349 024	−115.382 532	−115.380 681	−115.416 830	0.037 669
ΔE_r/kJ mol^{-1}	−7.09	−16.53	−11.75	−24.48	−14.26	−23.55	1.87
$\Delta_r H^{\ominus}$/kJ mol^{-1}	−5.22	−14.66	−9.88	−22.61	−12.39	−21.68	N/A
$\Delta E^{\ddagger}$/kJ mol^{-1}	41.38	34.03	41.05	32.07	40.82	31.31	−2.82
$E_a°$/kJ mol^{-1}	38.56	31.21	38.23	29.25	38.00	28.49	N/A

[a] Energy units are in Hartrees in the upper half of the table and in kJ mol^{-1} in the lower half. [b] Includes the multireference Davidson correction to the energy for size consistency. [c] Calculated at the MP2/cc-pvdz level.

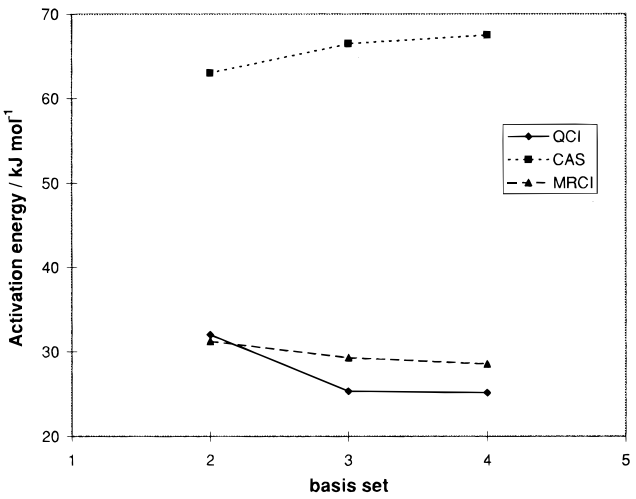

Figure 2. Plot of the convergence of the value of the activation energy with increasing basis set size (2 = cc-pvdz, 3 = cc-pvtz, 4 = cc-pvqz basis set). QCI is a QCISD(T)/cc-pvqz calculation, CAS is a 14-in-12 CASSCF/cc-pvqz calculation, and MRCI is an MR-CISD/cc-pvqz calculation using orbitals from a 6-in-6 CASSCF/cc-pvqz.

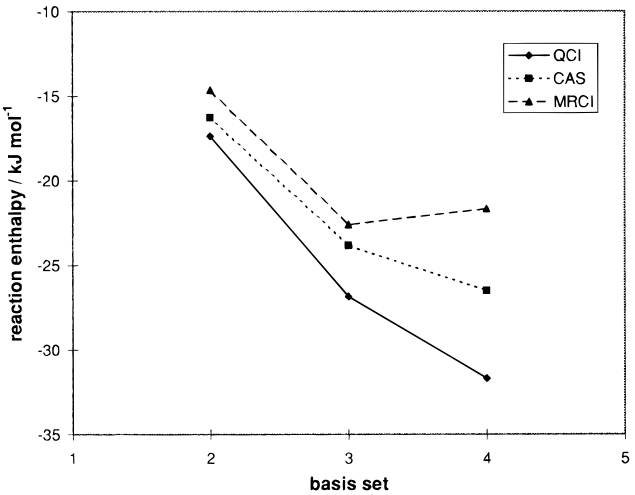

Figure 3. Plot of the convergence of the value of the reaction enthalpy with increasing basis set size (2 = cc-pvdz, 3 = cc-pvtz, 4 = cc-pvqz basis set). Abbreviations as in Figure 2.

Tables 4 and 5), which also include up to fourth-order excitations through the perturbation method. At the QCISD(T) level of theory an activation energy of $E_a° = 25.15$ kJ mol^{-1} is predicted, after correcting for the difference in zero-point vibrational energies between the reactants and the transition-state geometry. This activation energy is sufficiently low to ensure that the triplet abstraction pathway will make an important contribution to the overall reaction rates at higher temperatures. Table 5 shows that the QCISD(T) values for the activation energy are converged to within 0.2 kJ mol^{-1}.

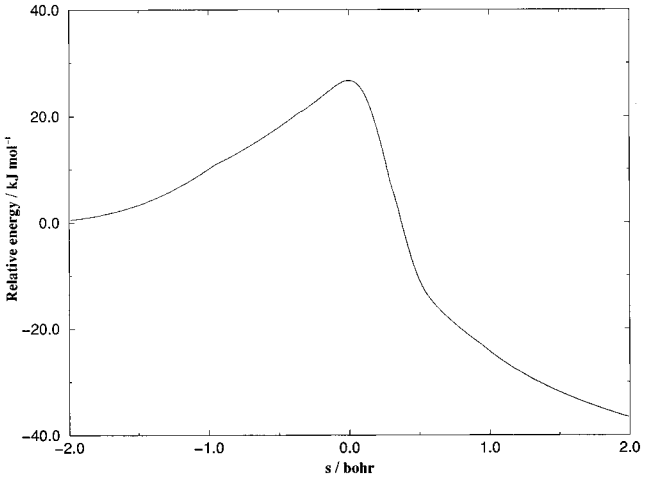

Figure 4. Minimum-energy path (MEP) for $CH_3 + OH \rightarrow {}^3CH_2 + H_2O$ calculated at the MP2/cc-pvdz level of theory.

Of the three methods (QCISD(T), CASSCF, and MR-CISD) the QCISD(T) gives the lowest value for the enthalpy of reaction. The predicted value at this level of theory, $\Delta_r H^{\ominus} = -31.69$ kJ mol^{-1} (see Table 5), is less than the best current estimates for this quantity (−38.0 kJ mol^{-1}). The uncertainty in the computed enthalpy of reaction is mainly due to the fact that our current calculations have been restricted to using a cc-pvqz basis. It may be seen from Figure 3 that the value of the reaction enthalpy has not yet fully converged with respect to the size of the basis. Further calculations with still larger basis sets would be required to obtain a value for the reaction enthalpy that is comparable with the experimental value. Given that the activation energy for the reaction is well-converged with respect to the basis set size, and that it is this quantity which determines the rate of reaction, we have not sought to carry out calculations with even larger basis sets so as to compute an accurate reaction enthalpy. The reaction enthalpy is in any case a well-known quantity and nothing new would be learned from such further calculations. It is reasonable to assume that the problems in converging the calculated value of the reaction enthalpy arises from the well-known difficulties in performing reliable calculations for the $^3CH_2$ species. It has been shown[17] that very high levels of theory and large basis sets are required to accurately obtain the enthalpy of formation of this system.

3. Reaction-Path Dynamics

3.A. Transition-State Theory (TST). Conventional transition-state theory calculations using the ab initio data were carried out using two programs: Polyrate 7.0[28] and TheRate 96.[29] Geometries, gradients, and Hessian (second-derivative) matrices calculated at the MP2/cc-pvdz level and energies calculated at the QCISD(T)/cc-pvqz level for the reactants, products, and transition state were used in the calculations.

TABLE 8: Calculated Rate Constants for the $CH_3 + OH \rightarrow {}^3CH_2 + H_2O$ Reaction[a]

T (K)	TST	TST/ZCT	TST/SCT	VTST	VTST/ZCT	VTST/SCT
200	1.26×10^{-18}	5.12×10^{-18}	1.39×10^{-17}	1.23×10^{-18}	4.97×10^{-18}	1.35×10^{-17}
250	2.34×10^{-17}	5.13×10^{-17}	9.84×10^{-17}	2.27×10^{-17}	4.94×10^{-17}	9.47×10^{-17}
298.15	1.59×10^{-16}	2.64×10^{-16}	4.19×10^{-16}	1.54×10^{-16}	2.53×10^{-16}	4.00×10^{-16}
300	1.70×10^{-16}	2.79×10^{-16}	4.40×10^{-16}	1.63×10^{-16}	2.67×10^{-16}	4.20×10^{-16}
400	2.18×10^{-15}	2.80×10^{-15}	3.62×10^{-15}	2.08×10^{-15}	2.65×10^{-15}	3.43×10^{-15}
600	3.56×10^{-14}	3.89×10^{-14}	4.37×10^{-14}	3.32×10^{-14}	3.49×10^{-14}	3.91×10^{-14}
800	1.78×10^{-13}	1.86×10^{-13}	1.98×10^{-13}	1.64×10^{-13}	1.65×10^{-13}	1.76×10^{-13}
1000	5.43×10^{-13}	5.54×10^{-13}	5.77×10^{-13}	4.93×10^{-13}	4.90×10^{-13}	5.11×10^{-13}
1200	1.26×10^{-12}	1.27×10^{-12}	1.31×10^{-12}	1.14×10^{-12}	1.12×10^{-12}	1.15×10^{-12}
1400	2.46×10^{-12}	2.47×10^{-12}	2.53×10^{-12}	2.21×10^{-12}	2.18×10^{-12}	2.23×10^{-12}
1600	4.30×10^{-12}	4.30×10^{-12}	4.37×10^{-12}	3.84×10^{-12}	3.78×10^{-12}	3.84×10^{-12}
1800	6.89×10^{-12}	6.88×10^{-12}	6.97×10^{-12}	6.15×10^{-12}	6.05×10^{-12}	6.13×10^{-12}
1900	8.51×10^{-12}	8.50×10^{-12}	8.60×10^{-12}	7.58×10^{-12}	7.46×10^{-12}	7.55×10^{-12}
2000	1.04×10^{-11}	1.04×10^{-11}	1.05×10^{-11}	9.23×10^{-12}	9.09×10^{-12}	9.18×10^{-12}
2050	1.14×10^{-11}	1.14×10^{-11}	1.15×10^{-11}	1.01×10^{-11}	9.98×10^{-12}	1.01×10^{-11}
2100	1.25×10^{-11}	1.25×10^{-11}	1.26×10^{-11}	1.11×10^{-11}	1.07×10^{-11}	1.08×10^{-11}
2150	1.36×10^{-11}	1.36×10^{-11}	1.37×10^{-11}	1.21×10^{-11}	1.17×10^{-11}	1.18×10^{-11}
2200	1.49×10^{-11}	1.48×10^{-11}	1.50×10^{-11}	1.32×10^{-11}	1.27×10^{-11}	1.28×10^{-11}
2250	1.62×10^{-11}	1.61×10^{-11}	1.63×10^{-11}	1.43×10^{-11}	1.38×10^{-11}	1.39×10^{-11}

[a] The rate constants are given in units of $cm^3\ s^{-1}$. The numbers should be multiplied by Avogadro's number to change to units of $mol^{-1}\ cm^3\ s^{-1}$. Abbreviations are as indicated in text.

3.B. Variational Transition-State Theory with Interpolated Corrections (VTST-IC). The calculation of a VTST rate constant[19] requires Hessian matrices at a number of points along the reaction path. If high-level ab initio electronic structure theory, such as QCISD(T) or MP4, is used to obtain these data, the calculations become prohibitively expensive. An alternative is to calculate the Hessian data along the minimum-energy path (MEP) at a lower, but still reasonable, level of theory and to calculate the energy at the top of the reaction barrier at a higher level of theory. The energy along the MEP is then interpolated so that it gives the correct energy at the transition-state geometry. This procedure obviates the need to calculate Hessians at very high levels of theory and is implemented in Polyrate 7.0, where it is known as VTST-IC.[30]

The points along the MEP were obtained from a Gaussian IRC calculation in which the reaction path was followed out to a distance of $s = 2.0\ a_0$ in both directions (in a mass-weighted coordinate system). Hessians were obtained at each of 125 points (spaced at 0.01 and 0.05 $amu^{1/2}\ a_0$) on the MEP at the MP2/cc-pvdz level of theory. Hessians for the reactants, transition state, and products were also calculated at this level. The classical reaction barrier and energy were obtained at the QCISD(T)/cc-pvqz level of theory using the MP2/cc-pvdz geometries of the reactants, transition state, and products. The interpolated energy profile, as generated by Polyrate using the VTST-IC method, along the calculated MEP is shown in Figure 4.

3.C. Tunneling Corrections. Reactions that involve the abstraction of small atoms such as hydrogen are known to be strongly affected by quantum tunneling. To take account of this in our calculations, two tunneling corrections to the transmission coefficient κ have been used. The first method is zero-curvature tunneling (ZCT[31]), in which the correction is calculated for one-dimensional motion along the reaction coordinate (MEP), with the other degrees of freedom remaining adiabatic along the reaction path. This method is also known as the statistical adiabatic ground-state method, or MEP−SAG. The second method is small-curvature tunneling (SCT[32]), in which the tunneling path is calculated by including the curvature of the MEP. It would have been desirable to also calculate large-curvature tunneling probabilities, but the Polyrate code was unable to do this from our electronic structure data.

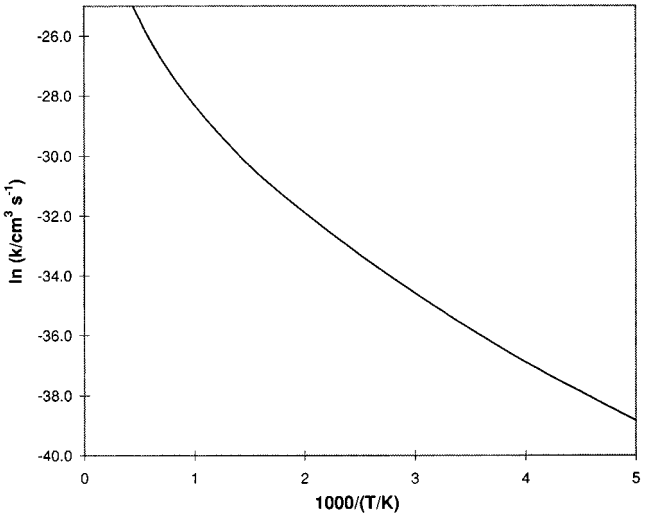

Figure 5. Arrhenius plot for rate constants calculated using variational transition-state theory with small-curvature tunneling (VTST/SCT)

3.D. Results. Table 8 contains the rate constants calculated from the ab initio data with all the methods outlined above. The geometry of the generalized transition state calculated using VTST theory is quite close to the ab initio saddle point ($s = -0.02$ at 300 K) on the MEP; consequently, the traditional transition-state theory (TST) and variational transition-state theory (VTST) rate constants are quite similar at all temperatures. The table shows that the inclusion of tunneling has a significant effect on the value of the rate constant, especially at lower temperatures. This is seen by comparing columns 2 and 4 (TST and TST/SCT) and columns 5 and 7 (VTST and VTST/SCT). Nevertheless, the reaction can be expected to be slow under ambient conditions, with $k^{298} = 4.0 \times 10^{-16}\ cm^3\ s^{-1}$ (VTST/SCT value). An Arrhenius plot based on the VTST/SCT results is shown in Figure 5. The curvature of the plot over this extended range of temperature can be explained by the temperature dependence of the partition functions. At temperatures greater than 1000 K in methane flames, the reaction of CH_3 with OH to form $^3CH_2$ and H_2O can be expected to play a role in the overall combustion cycle.

A comparison of our result with some other results derived for both the reaction to give $^1CH_2$ and the reaction to give $^3CH_2$ is shown is Figure 6. As mentioned above, the only other data

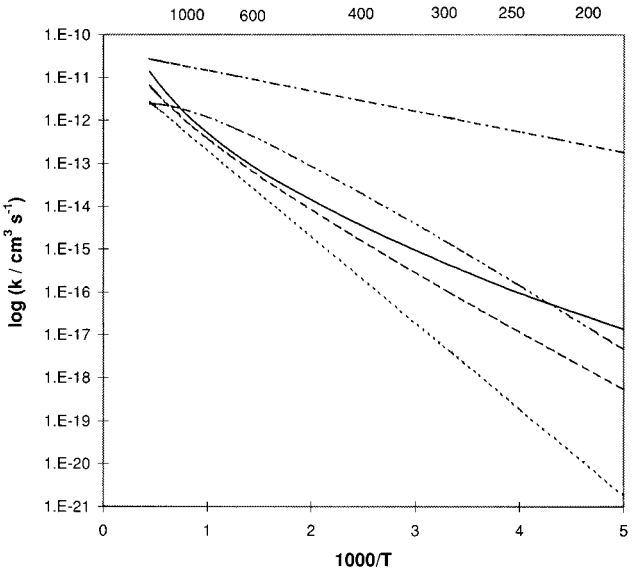

Figure 6. Arrhenius plot showing a comparison of our calculated rate constants (VTST/SCT column of Table 8) with other theoretical and experimental work: —••—, $^1CH_2$, Dean et al., ref 1, see text; —•—, Grotheer et al., refs 9 and 10; •••, $^3CH_2$, Dean et al., ref 1, see text; - - -, GRI-Mech reaction scheme, ref 33; —, present work.

calculated for this reaction on the triplet surface were given in Dean and Westmoreland. It is unclear from their work precisely how they obtain their rate expression. However, the line shown in Figure 6 reproduces the result in their paper approximately. One other rate expression is available, which was estimated from data on the hydrogen abstraction from CH_4 by OH. This expression is used in the GRI-Mech[33] reaction scheme for CH_4 oxidation. The two results for $^1CH_2$ are from Dean and Westmoreland[1] calculations and Grotheer and co-workers' experimental data.[9,10] Dean and Westmoreland's are QRRK calculations based on the experimental data of Hatakeyama et al.[34] We have used the rate expression and parameters given in Table 1 of ref 1 for an Ar collision partner at 760 Torr. Our results for the triplet surface agree reasonably well with the GRI-Mech[33] estimate, especially at high temperature. There is also reasonable agreement with Dean and Westmoreland's estimate at high temperatures. It is noteworthy that Grotheer's experimental results for the singlet reaction show that it is faster than the triplet reaction at all temperatures. This is not surprising given that the reaction on the singlet surface has no barrier.

Furthermore, Grotheer et al.'s results probably refer to a combination of the rates for production of singlet and triplet CH_2 as their experimental technique does not distinguish between them. The experiments were only done over a temperature range of 300−700 K, so the extrapolation to both lower and higher temperatures is open to question.

4. Conclusions

Good-quality ab initio and variational transition-state theory calculations have been performed on the $CH_3 + OH \rightarrow {}^3CH_2 + H_2O$ reaction proceeding on a potential energy surface associated with a triplet-symmetry spin state of the system. Unlike the surface associated with singlet-spin symmetry, the reaction on the triplet surface produces ground-state products. The calculations show that the reaction has an appreciable barrier of 25.15 kJ mol^{-1} at 0 K and would therefore be slow at low temperatures (i.e. ∼300 K). Most experimental investigations of the $CH_3 + OH \rightarrow CH_2 + H_2O$ reaction have not distinguished between production of singlet or triplet methylene. At the temperatures found in methane flames, our results indicate that reaction via the triplet surface will make an important contribution to the overall rate. The analytic expression

$$k = (1.848\,338 \times 10^{-21})T^3 \exp(-1400 \pm 213/T)\ \mathrm{cm^3\ s^{-1}}$$

$$(\text{or } k = (1.113\,272 \times 10^{-4})T^3 \exp(-1400 \pm 213/T)\ \mathrm{dm^3\ mol^{-1}\ s^{-1}})$$

provides a good fit to our computed rate constants over the whole temperature range 200−2250 K (see last column of Table 8). The estimate of the margin of error in the equation is based on an uncertainty of about 0.8 kJ mol^{-1} associated with an uncertainty in the precise geometry of the transition state. This uncertainty was itself determined by performing additional QCISD calculations for the location of the transition-state geometry. There is a further uncertainty of 0.2 kJ mol^{-1} arising from incomplete basis set convergence (see Table 5). For safety we have doubled these error margins to yield an uncertainty of 2 kJ mol^{-1} in the activation energy. We have then recomputed the rates of reaction and estimated the uncertainty in the analytic expression for the rate constant from this.

The authors thank the EPSRC for financial support. They also thank the Computational Chemistry Working Party for computer time on the Columbus computer at the Rutherford Appleton Laboratory, which was also provided under a grant from the EPSRC. They thank Dr. D. B. Smith for encouraging them to undertake this work and for many fruitful discussions. They also thank Dr. M. J. Brown of British Gas for useful discussions.

References and Notes

(1) Dean, A. M.; Westmoreland, P. R. *Int. J. Chem. Kinet.* **1987**, *19*, 207.
(2) Walch, S. P. *J. Chem. Phys.* **1993**, *98*, 3163.
(3) Bauschlicher, C. W., Jr.; Langhoff, S. R.; Walch, S. P. *J. Chem. Phys.* **1992**, *96*, 450.
(4) Harding, L. B.; Schlegel, H. B.; Krishnan, R.; Pople, J. A. *J. Phys. Chem.* **1980**, *84*, 3394.
(5) Just, Th. *Twenty-Fifth Symposium (International) on Combustion*; The Combustion Institute, Pittsburgh, PA, 1994; p 687.
(6) Hack, W.; Wagner, H. Gg.; Wilms, A. *Ber. Bunsen-Ges. Phys. Chem.* **1988**, *92*, 620.
(7) Hack, W.; Thiesemann, H. *J. Phys. Chem.* **1995**, *99*, 17364.
(8) Oser, H.; Stothard, N. D.; Humpfer, R.; Grotheer, H. H. *J. Phys. Chem.* **1992**, *96*, 5359.
(9) Oser, H.; Stothard, N. D.; Humpfer, R.; Grotheer, H.-H.; Just, Th. *Twenty-Fourth Symposium (International) on Combustion*; The Combustion Institute: Pittsburgh, PA, 1992; p 597.
(10) Humpfer, R.; Oser, H.; Grotheer, H.-H.; Just, Th. *Twenty-Fifth Symposium (International) on Combustion*; The Combustion Institute: Pittsburgh, PA, 1994; p 721.
(11) Sworski, T. J.; Hochanadel, C. J.; Orgen, P. J. *J. Phys. Chem.* **1980**, *84*, 129.
(12) Anastasi, C.; Beveton, S.; Ellermann, T.; Pagsberg, P. *J. Chem. Soc., Faraday Trans.* **1991**, *87*, 2325.
(13) Hughes, K. J.; Pereira, A. R.; Pilling, M. J. *Ber. Bunsen-Ges. Phys. Chem.* **1992**, *96*, 1352.
(14) Chase, M. W., Jr.; Davies, C. A.; Downey, J. R.; Frurip, D. J.; MacDonald, R. A.; Syverud, A. N. JANAF Thermochemical Tables. *J. Phys. Chem. Ref. Data (Suppl.)* **1985**, *14*.
(15) Baulch, D. L.; Cox, R. A.; Crutzen, P. J.; Hampson, R. F., Jr.; Kerr, J. A.; Troe, J.; Watson, R. T. *J. Phys. Chem. Ref. Data* **1982**, *11*, 493.
(16) Dóbé, S.; Bérces, T.; Turányi, T.; Márta, F.; Grussdorf, J.; Temps, F.; Wagner, H. Gg. *J. Phys. Chem.* **1996**, *100*, 19864.
(17) Doltsinis, N. L.; Knowles, P. J. *J. Chem. Soc., Faraday Trans.*, in press.
(18) Jensen, P.; Bunker, P. R. *J. Chem. Phys.* **1988**, *89*, 1327.
(19) See, for example: Truong, T. N.; Duncan, W. T.; Bell, R. L. *ACS Symp. Ser.* **1996**, *629*, 85.
(20) Frisch, M. J.; Trucks, G. W.; Schlegel, H. B.; Gill, P. M. W.; Johnson, B. G.; Robb, M. A.; Cheeseman, J. R.; Keith, T.; Petersson, G. A.; Montgomery, J. A.; Raghavachari, K.; Al-Laham, M. A.; Zakrzewski,

V. G.; Ortiz, J. V.; Foresman, J. B.; Cioslowski, J.; Stefanov, B. B.; Nanayakkara, A.; Challacombe, M.; Peng, C. Y.; Ayala, P. Y.; Chen, W.; Wong, M. W.; Andres, J. L.; Replogle, E. S.; Gomperts, R.; Martin, R. L.; Fox, D. J.; Binkley, J. S.; Defrees, D. J.; Baker, J.; Stewart, J. P.; Head-Gordon, M.; Gonzalez, C.; Pople, J. A. *Gaussian 94*, Revision D.4, Gaussian, Inc.: Pittsburgh, PA, 1995.

(21) MOLPRO is a package of ab initio programs written by H.-J. Werner and P. J. Knowles with contributions from J. Almlöf, R. D. Amos, A. Berning, M. J. O. Deegan, F. Eckert, S. T. Elbert, C. Hampel, R. Lindh, W. Meyer, A. Nicklass, K. Peterson, R. Pitzer, A. J. Stone, P. R. Taylor, M. E. Mura, P. Pulay, M. Schuetz, H. Stoll, T. Thorsteinsson, and D. L. Cooper, 1996.

(22) Møller, C.; Plesset, M. S. *Phys. Rev.* **1934**, *46*, 618.

(23) Woon, D. E.; Dunning, T. H. *J. Chem. Phys.* **1993**, *98*, 1358. Dunning, T. H. *J. Chem. Phys.* **1989**, *90*, 1007.

(24) Krishnan, R.; Binkley, J. S.; Seeger, R.; Pople, J. A. *J. Chem. Phys.* **1980**, *72*, 650.

(25) Pople, J. A.; Head-Gordon, M.; Raghavachari, K. J. *J. Chem. Phys.* **1987**, *87*, 5968.

(26) See: Werner, H.-J.; Knowles, P. J. *J. Chem. Phys*. **1985**, *82*, 5053. Knowles, P. J.; Werner, H.-J. *Chem. Phys. Lett*. **1985**, *115*, 259. See also: Werner, H.-J.; Meyer, W. *J. Chem. Phys.* **1980**, *73*, 2342. Werner, H.-J.; Meyer, W. *J. Chem. Phys*. **1981**, *74*, 5794.

(27) See: Werner, H.-J.; Knowles, P. J. *J. Chem. Phys*. **1988**, *89*, 5803. Knowles, P. J.; Werner, H.-J. *Chem. Phys. Lett*. **1988**, *145*, 514. See also: Werner, H.-J.; Reinsch, E. A. *J. Chem. Phys*. **1982**, *76*, 3144. Werner, H.-J. *Adv. Chem. Phys*. **1987**, *LXIX*, 1.

(28) Steckler, R.; Chuang, Y.-Y.; Coitiño, E. L.; Hu, W.-P.; Liu, Y.-P.; Lynch, G. C.; Nguyen, K. A.; Jackels, C. F.; Gu, M. Z.; Rossi, I.; Fast, P.; Clayton, S.; Melissas, V. S.; Garrett, B. C.; Isaacson, A. D.; Truhlar, D. G. *POLYRATE*, version 7.0; University of Minnesota: Minneapolis, MN, 1996.

(29) Truong, T. H.; Duncan, W. T. *TheRate 96*; University of Utah.

(30) Hu, W.-P.; Liu, Y.-P.; Truhlar, D. G. *J. Chem. Soc., Faraday Trans.* **1994**, *90*, 1715.

(31) Truhlar, D. G.; Isaacson, A. D.; Garrett, B. C. Generalised Transition State Theory. In *The Theory of Chemical Reaction Dynamics*; Baer, M., Ed.; CRC Press: Boca Raton, FL, 1985; Vol. 4, Chapter 2, pp 65−137.

(32) See: Lu, D.-H.; Truong, T. N.; Melissas, V. S.; Lynch, G. C.; Liu, Y.-P.; Garrett, B. C.; Steckler, R.; Isaacson, A. D.; Rai, S. N.; Hancock, G.; Lauderdale, J. G.; Joseph, T.; Truhlar, D. G. *Comput. Phys. Commun.* **1992**, *71*, 235. Liu, Y.-P.; Lynch, G. C.; Truong, T. N.; Lu, D.-H.; Truhlar, D. G. *J. Am. Chem. Soc*. **1993**, *115*, 2408.

(33) Bowman, C. T.; Hanson, R. K.; Davidson, D. F.; Gardiner, W. C., Jr.; Lissianski, V.; Smith, G. P.; Golden, D. M.; Frenklach, M.; Goldenberg, M. GRI-Mech 2.11 data base; http://www.me.berkeley.edu/gri_mech/.

(34) Hatakeyama, S.; Bandow, H.; Okuda, M.; Akimoto, H. *J. Phys. Chem*. **1981**, *85*, 2249.